# Dielectric-breakdown threshold and nonlinear-refractive-index measurements with picosecond laser pulses*

W. L. Smith, J. H. Bechtel, and N. Bloembergen
*Gordon McKay Laboratory, Harvard University, Cambridge, Massachusetts 02138*
(Received 18 February 1975)

Single pulses from a well-calibrated mode-locked YAG:Nd laser have been used to study the dielectric-breakdown properties of 14 transparent solids. Results are presented for the breakdown threshold electric fields, accurate to an estimated 15%. The experimental technique permits simultaneous measurement of the nonlinear susceptibility $\chi_{xxxx}^{(3)}(-\omega,\omega,\omega,-\omega)$, via the nonlinear refractive index. Susceptibility results with estimated accuracy of 50% are presented.

## I. INTRODUCTION

It is well known that damage to transparent optical components in high-power laser systems constitutes a limiting factor to their performance. In many practical cases the damage threshold is set by the presence of absorbing inclusions, or by the occurrence of self-focusing. It has, however, been established that an intrinsic damage threshold, characteristic of the bulk transparent material, can be defined. If the effects of inclusions have been eliminated, and if one has corrected for the effects of self-focusing, the threshold is determined by the onset of avalanche ionization, in a manner which is very similar to low-frequency electric breakdown.[1] Since the conduction-electron density has to build up from the initial density of about $10^8$ to $10^{10}$ electrons/cm$^3$ to a critical value of about $10^{18}$ electrons/cm$^3$ during the duration of the laser pulse, the damage threshold has a characteristic dependence on pulse duration. Most available experimental data were taken with pulses of nanoseconds or longer duration. In fact, heretofore, there was only one quantitative datum point taken with a picosecond pulse.[2] The reliability of that point has been questioned on the grounds that, for picosecond pulses, impurities of submicroscopic size may play a dominant role and that no morphological study of the damaged region had been made. The purpose of this paper is to provide systematic picosecond data on the damage threshold in 14 transparent materials. The data obtained are characteristic of the material and are very reproducible.

It is necessary to take into account the effects of self-focusing in this experiment, even though the maximum pulse power was always less than the critical power for self-focusing.[3,4] This power $P_{cr}$ is related to the intensity-dependent contribution to the index of refraction $n_2$, where

$$n = n_0 + n_2 |E_{rms}|^2 , \tag{1}$$

by

$$P_{cr} = c\lambda^2/32\pi^2 n_2 . \tag{2}$$

In the above equations, $n_0$ is the linear refractive index, $c$ is the speed of light, and $\lambda$ is the vacuum wavelength. Wagner *et al.*[5] discuss the deformation of a Gaussian light pulse by the self-interaction represented by Eq. (1). Let $w_1$ be the beam waist, i.e., the radius at which the intensity drops to $1/e$ of its on-axis value, at low power levels. Then the low-power focal area $\pi w_1^2$ is reduced by a factor $(1 - P/P_{cr})$ due to self-action. The maximum intensity is consequently increased by a factor $(1 - P/P_{cr})^{-1}$. Zverev and Pashkov[6] and Fradin[7] have suggested how this effect may be used to determine $P_{cr}$, and consequently $n_2$, by measuring the damage threshold as a function of focal length, utilizing different lenses.

Consider a low-power diffraction-limited Gaussian pulse with an initial $1/e$ intensity radius $\rho$. A lens, without spherical aberration and with focal length $f$, will produce a focal spot with a radius (to the $1/e$ intensity point) of

$$w_1 = \lambda f/2\pi\rho . \tag{3}$$

If the pulse total power is $P$ and we define an area $A = \pi w_1^2$, the focal plane intensity distribution is given by

$$I(r) = (P/A)\, e^{-(r/w_1)^2} . \tag{4}$$

For high-power pulses where self-focusing tendencies cannot be ignored, the relationship between the maximum intensity and the power becomes

$$I_{max} = (P/A)(1 - P/P_{cr})^{-1} \tag{5}$$

or

$$P^{-1} = I_{max}^{-1} A^{-1} + P_{cr}^{-1} . \tag{6}$$

If one plots, therefore, the reciprocal measured power, necessary to produce the value of $I_{max}$ required for breakdown, as a function of the reciprocal focal area $A^{-1}$, one should obtain a straight line. The slope of this straight line gives the breakdown

rms electric field strength

$$E_b = (I_{max}/cn_0\epsilon_0)^{1/2}, \quad (7)$$

where $\epsilon_0$ is the free-space permittivity. The intercept with the vertical axis determines $P_{cr}$ and $n_2$.

One restriction implicit in the preceding discussion concerns the response time of the self-focusing mechanism. Various mechanisms for self-focusing exist,[3,8] with response times from the order of $10^{-8}$ sec for electrostrictive and thermal self-focusing, to the order of $10^{-15}$ sec for self-focusing originating in the electronic hyperpolarizability. For picosecond-pulse experiments in solids, the only mechanism fast enough to reach its steady-state value is the electronic hyperpolarizability. That mechanism follows our laser-pulse intensity essentially instantaneously, and so the assumption of a steady-state nonlinearity is a valid one for our experiment. Indeed, picosecond pulses provide results free from ambiguity introduced by slower contributions to $n_2$, an ambiguity which may hinder $Q$-switched laser-pulse experiments.

The method described above has been used to measure the rms breakdown field strength $E_b$ and the critical power for self-focusing $P_{cr}$ in several transparent solids of interest. Section II describes the experimental apparatus and procedure, including a technique for measuring the product of the laser-pulse duration and pulse area on a shot-to-shot basis in a simple manner. Results are presented and discussed in Sec. III.

## II. EXPERIMENTAL METHOD

### A. Laser system

A mode-locked YAG: Nd laser system generated the picosecond pulses used in these experiments. The experimental arrangement is illustrated in Fig. 1. A 6-mm-diam by 3-in-long Brewster-ended YAG: Nd rod supplies gain. Mode locking is achieved by a contacted dye cell which confines a 0.5-mm-thick sheet of flowing Kodak 9860 saturable absorber. $TEM_{00}$ transverse profile is established with an intracavity aperture. Single-pulse switch-out is effected by a cylindrical-ring electrode potassium dideuterium phosphate Pockels cell, positioned between crossed polarizers, and pulsed by a nitrogen-filled high pressure laser-triggered spark gap. A selected pulse then propagates through two single-pass YAG: Nd amplifiers for augmentation of energy. A repetition rate of 20 pulses/sec is available, and an amplified single-pulse peak power exceeding 300 MW has been measured. CRO-1 is a Tektronix 519 oscilloscope used in conjunction with high-speed biplanar photodiode PD-1 (ITT F4000, S-1 response), for single-pulse monitoring. Two Glan polarizers form the variable attenuator A in Fig. 1. The calibrated photodiode PD-3 (S-1 response) measures the energy incident on the lens. The second-harmonic generation channel, ending with photodiode PD-2 (S-20 response), is used with PD-3 to obtain single-pulse values of the product of the pulse duration and pulse area, as will be described later. CRO-2 is a Tektronix 555 dual-beam oscilloscope. In Fig. 1, L represents the focusing lens and S the sample materials tested in the experiments.

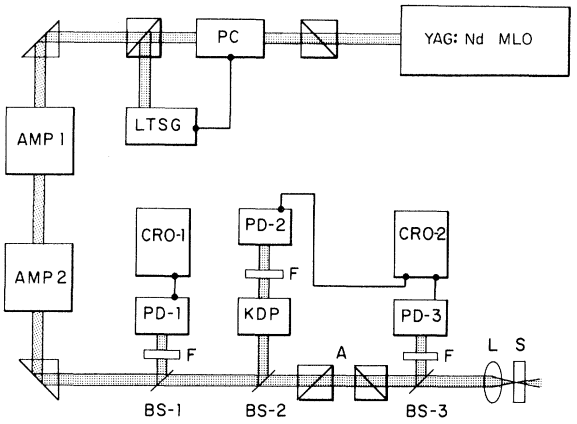


FIG. 1. Schematic diagram of the experimental arrangement. MLO, mode-locked YAG: Nd oscillator; PC, Pockels cell; LTSG, laser-triggered spark gap; AMP, YAG: Nd amplifier; BS, beam splitter; F, filter; PD, biplanar photodiode; CRO, oscilloscope; KDP, second-harmonic generation crystal; A, Double Glan-prism variable attenuator; L, focusing lens; S, dielectric sample.

### B. Pulse characteristics

#### *1. Spatial characteristics*

Since precise measurement of threshold optical electric fields requires an accurate knowledge of both the spatial and temporal pulse shape and the pulse energy, great care was taken toward those measurements.

At the actual site on the optical table where the focusing lens was later placed for the breakdown measurements, three scans across the beam were made with a 50-$\mu$m pinhole to determine the transverse intensity distribution. The results of one of the scans is shown in Fig. 2. In addition, pictures were taken of phase-matched second-harmonic light with a multilens camera[9] (MLC). The result of each of the above tests was that the intensity distribution is of Gaussian form to at least the $1/e^2$ points, and that the average $1/e$ intensity radius $\langle\rho\rangle$ is $1.1 \pm 0.1$ mm.

#### *2. Temporal characteristics*

In order to determine the temporal pulse profile of the output, two techniques[10] were used: a second-harmonic-generation autocorrelation method

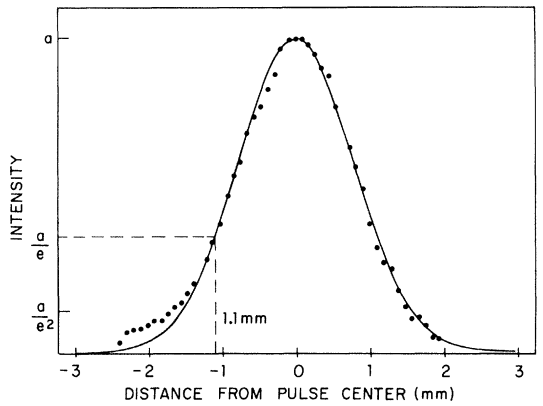


FIG. 2. Intensity distribution of laser pulse at location of focusing lens. The solid line is a Gaussian fit to the data, yielding a $1/e$ intensity radius 1.1 mm.

(SHAC), and two-photon-fluorescence (TPF) photography. The two methods are formally equivalent, both providing $1+2G_2(\tau)$. In either method, a single pulse is split into two pulses of equal amplitude (any disparity in the two amplitudes degrades the contrast ratio). In the TPF arrangement, the two pulses are then redirected by mirrors to overlap in a precisely collinear fashion within a two-quantum-absorptive material such as Rhodamine 6G, and the dye fluorescence is photographed. In the SHAC method the beam splitter is part of a Michelson interferometer. The pulses are recombined collinearly, after one has been delayed by a variable amount, and directed through a potassium dihydrogen phosphate (KDP) crystal. One plots second-harmonic output as a function of delay. The result of one of the SHAC runs is shown in Fig. 3. The enhanced scatter of the points near the center of the graph is due to interference effects in the interferometer. The curve is a four-parameter least-squares fit to the function $K_1+K_2\exp[-2(z-\frac{1}{2}z_0)^2/c^2\tau^2]$. It shows a contrast ratio [equal to $(K_1+K_2)/K_1$] of 2.7:1. The results of TPF traces, each one the result of many laser shots, agree with the data of Fig. 3: the average full-width-at-half-maximum (FWHM) temporal duration of the laser output is $30.0\pm6.0$ psec, implying an average $1/e$ half-duration $\langle\tau\rangle$ of $18.0\pm3.6$ psec.

### 3. *Individual-pulse $\tau$, $A$ measurements*

During the course of the laser calibration, a narrow distribution of individual pulse durations was actually observed, the average of which is the value stated above. In order to investigate the pulse-width statistics further, and to be able to obtain individual $\tau$ measurements, a simple pulse-duration–pulse-area monitor system was devised and added to the laser system.[11] The rationale of this monitor system follows from the proven Gaussian spatial and temporal distribution of the pulse intensity. Let $\mathcal{E}_f$ be the energy content of the sample of the fundamental pulse that is measured by photodiode PD-3 in Fig. 1, and $\mathcal{E}_{sh}$ be the energy content of the second-harmonic sample that is measured by PD-2. Then, for small harmonic conversion efficiencies, it can be shown that

$$\mathcal{E}_f^2/\mathcal{E}_{sh}=q\tau A\ , \tag{8}$$

where $q$ is a collection of constants for a given experiment. If, in the course of an experiment, enough data points are taken so that the average of the ratio values given above is meaningful and representative, then that average value can be set equal to the product of the known, previously measured average values, $\langle\tau\rangle\langle A\rangle$, thereby calibrating absolutely the individual pulse values of the ratio given by Eq. (8). Using these individual-pulse values of $\tau A$, one obtains individual-pulse intensity values from the easily measured pulse-energy values. This simple scheme is useful in obtaining accurate data for processes which are highly nonlinear in the intensity, such as laser-induced breakdown or multiphoton photoemission.[12]

### C. Focal considerations

As discussed in Sec. I, a plot of the reciprocal breakdown power versus reciprocal focal area yields the breakdown field and the nonlinear refractive index. For each material tested in these experiments, the breakdown power was measured for three different lenses. The focal lengths were 0.5, 1.0, and 1.5 in. All were of proper shape to minimize spherical aberration.[13] In the absence of all aberration, the intensity distribution in the focal plane inside the test material would be the Fourier

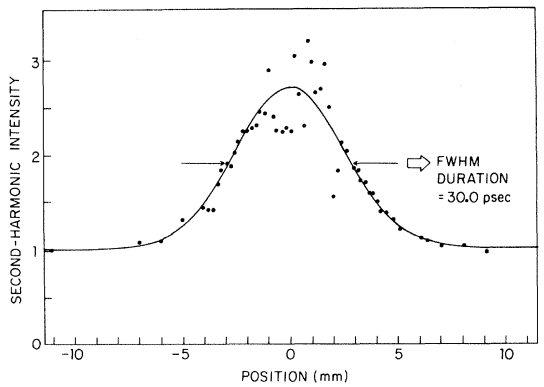


FIG. 3. Results of measurement of the laser pulse average temporal duration, using a second-harmonic-generation technique. The enhanced scatter of the points in the middle of the data is due to interference effects in the interferometer. The solid curve is a least-squares fit to the data, yielding a FWHM duration of 30.0 psec and a contrast ratio of 2.7:1.

transform of the distribution in the back focal plane of the lens. The latter is of the form $I(r) = I_0 \exp - (r/\rho)^2$, and so the focal-plane distribution would be $I_f(r) = I_0' \exp - (r/w_1)^2$, where $w_1$ is given in Eq. (3). Such performance would be diffraction limited. In reality, however, contributions to the focal radius due to spherical aberration by the lens and by the planar surface of the test material must be considered. The radius that would result from the first of these two aberrations $w_2$ is given by[13]

$$w_2 = 4\kappa\rho^3/f^2 , \tag{9}$$

where $\kappa$ is a function of lens refractive index and has the value 0.069 for the 0.5- and 1.5-in. focal-length lenses (quartz, $n_0 = 1.4498$), and 0.0455 for the 1-in. focal-length lens (glass, $n_0 = 1.6667$), at 1.06 $\mu$m. Equation (9) was derived for the case of a plane wave incident on the lens, but it is still useful here in a manner to be described below. The focal radius that would result from spherical aberration by the planar test material surface[14] $w_3$ is given by

$$w_3 = D(n_0^2 - 1)\rho^3/2n_0^3 f^3 , \tag{10}$$

where $D$ is the distance between the interface and the focal point and, in the experiments here, was always 2.0 mm. The effective focal radius $w$ is related to the above constituents by

$$w = (w_1^2 + w_2^2 + w_3^2)^{1/2} . \tag{11}$$

In Table I, the quantities introduced above are tabulated for the three lenses used here. Because of the shallow depth of focus $D$ maintained here, the contribution to $w$ from $w_3$ is seen to be less than 1% in all cases. The contribution from $w_2$ is also seen to be less than 1% for the $f = 1$-in. and $f = 1.5$-in. lenses. Thus, in these two cases, the use of Eq. (9) to compute $w_2$ is acceptable. For the $f = 0.5$-in. lens, however, the spherical aberration contribution to $w$ as calculated from Eq. (9) is nonnegligible. It was felt necessary to perform an experiment to determine the focal distribution for this lens. To that end a chromium-steel razor blade was mounted on a two-dimensional precision translator with 0.13-$\mu$m resolution. The front surface of the blade edge was then positioned precisely in the focal plane of the 0.5-in. focal-length lens, the focal plane being identified as that requiring the least irradiance to produce a spark on the blade surface. The blade was then swept in increments across the beam, and the fraction of the incident pulse energy (as measured by a reference detector) that was not blocked by the blade was measured as a function of position. Several shots were taken at each position, and the irradiance was always maintained below the blade damage level. A simple calculation shows that the transmission function $T(x)$ should be of the form

$$T(x) = (\pi w^2)^{-1} \int_{-\infty}^{x} \int_{-\infty}^{\infty} e^{-(x'^2+y^2)/w^2} \, dx' \, dy$$

$$= \tfrac{1}{2}[1 + \mathrm{erf}(x/w)] . \tag{12}$$

The experimental data conformed well to a curve of the above form if $w$ was given the value 3.3 $\mu$m. Microscopic examination of the blade edge after the experiment verified that it had not been disfigured. Therefore, the value of 3.3 $\mu$m for the focal radius for the $f = 0.5$-in. lens was used in all data analysis in this report, and it appears in Table I.

Finally, aberration due to decentration and tilt[15] of the lens must be considered. In these experiments, such further contributions to $w$ were rendered negligible by the following alignment procedure, which was used for every experiment. Firstly, in order to deal with tilt, the lenses were mounted in holders which allowed the attachment of a microscope slide in front of the lens in such a manner as to be parallel to the plane of the lens. Next the beam was apertured so as to allow only a small (0.5-mm-diam) central section to strike the attached slide. The lens was then adjusted to be normal to the propagation direction to within better than 1.0° by adjusting the holder so that the reflection was collinear with the pulse propagation direction. Secondly, decentration was made negligible by two operations. Before the lens was placed in the system, the position of the center of the laser pulse at a point past the lens site was located by a marked phosphorescent card. Then with the lens inserted, and corrected for tilt as discussed above, it was translated so that the center of the transmitted light was coincident with the position previously located. Additionally, the reflection of the pulse from the curved, first face of the lens was observed with another viewing card and when alignment was obtained, the reflection was symmetrically distributed about the propagation direction. The lenses could be centered to within 0.1 mm easily, making associated aberration negligible. The reproducibility of lens positioning afforded by the above simple techniques is necessary for accurate absolute breakdown field measurements over a large series of materials.

TABLE I. Focal parameters.

| Focal length $f$ (in.) | $w_1$ ($\mu$m) | $w_2$ ($\mu$m) | $w_3$ ($\mu$m) | $w$ ($\mu$m) | $A = \pi w^2$ ($\mu$m$^2$) |
|---|---|---|---|---|---|
| 0.5 | 1.95 | a | 0.23 | 3.3[a] | 34.2 |
| 1.0 | 3.80 | 0.37 | 0.03 | 3.94 | 48.2 |
| 1.5 | 5.85 | 0.25 | 0.01 | 5.85 | 107.9 |

[a]See text, Sec. II C.

### D. Procedure

To begin each experiment, the sample was optically polished and blown with dry nitrogen to remove any residual abrasive particles from the surface. The sample was then clamped onto an $x$-$y$ translator, and the entrance surface was aligned normal to the propagation direction. It was necessary to maintain a hot-air stream over the most hygroscopic of the materials to retain surface quality. The amplifier gain and the variable attenuator were then adjusted so that the approximate breakdown irradiance entered the material and so that sufficient signal was available for the $\tau A$ measurement devices, as discussed earlier. Thereafter, the attenuator was left unchanged in order that the ratio values of Eq. (8) retain their usefulness, as noted earlier. Any further fine adjustment of the input irradiance was done with the amplifier gain control. The material was translated between pulses so that a new portion of the material was probed by each pulse, and the coordinates of each probed location were recorded. A fast photodiode/Tektronix 519 oscilloscope combination (PD-1/CRO-1 in Fig. 1) was monitored during each firing in order to eliminate data from pulses with satellites. At each firing, the fundamental energy and the harmonic energy were recorded. Loss of energy by reflection from the lens and material surface was taken into account in each experiment. The fundamental energy was measured with a photodiode calibrated with an Eppley Laboratory thermopile. Breakdown sparks were initially detected with well dark-adapted eyes operating in a dark room shielded from laser flashlamp light. Later, using the recorded coordinates of the probed sites, the crystal was observed under a microscope to verify breakdown at any visually uncertain points. The observed damage was confined to a cylindrically shaped volume typically 2 $\mu$m in diameter and 25–50 $\mu$m in length, and therefore occupied a small fraction of the focal volume, just above threshold. The reproducibility of the data when probing different specimens and different volume elements within the same specimen indicate that a property characteristic of the bulk material is observed. Only a few isolated cases of inclusions were observed under the microscope, and they were eliminated. A further detailed account of the morphology of the damage will be given elsewhere. Typically, 50 shots were used near the threshold region with each lens for each material. The data were then plotted as shown in Fig. 4 for KCl. The sharpness of the threshold is typical of the behavior encountered in these experiments. The uncertainty in the breakdown energy was generally less than 10%. The three encircled points were associated with pulses having unusually short $\tau A$ values, and did cause breakdown even though their energy was below the threshold energy evident in the figure for pulses with $\tau A$ nearer to $\langle\tau\rangle\langle A\rangle$. The damage energy was determined in this manner in each case, and then $\langle\tau\rangle$ was used to convert the energy to power. A pulse energy $\mathcal{E}_f$ is related to the pulse power $P$ by $P=\mathcal{E}_f/(\pi)^{1/2}\tau$. The reciprocal damage-power values were then plotted versus reciprocal focal area as discussed in Sec. I. An example, that of KCl, is shown in Fig. 5. A least-squares fit to the three points then yields the desired quantities—the breakdown field $E_b$, independent of self-focusing effects, and the nonlinear index of refraction $n_2$, via the critical power for self-focusing.

## III. RESULTS

In this section results are presented from tests on 14 materials. All samples were obtained from

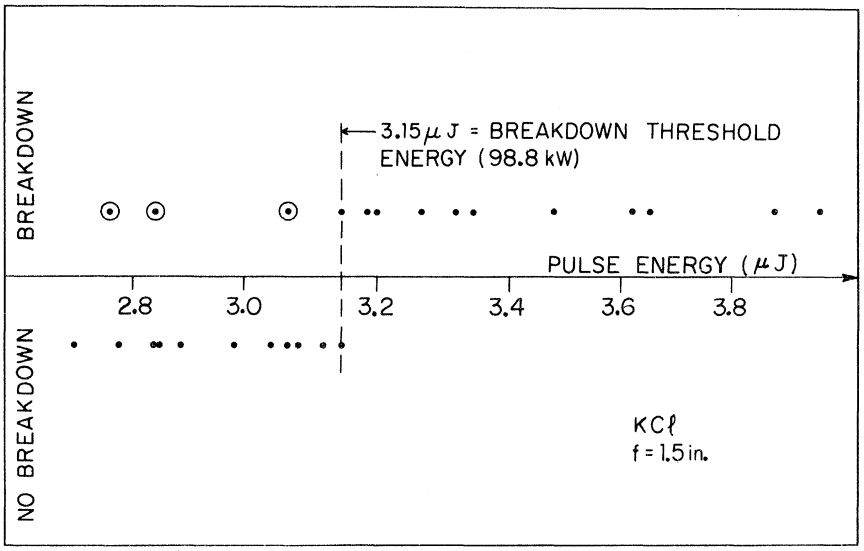


FIG. 4. Results of breakdown experiment in KCl for $f=1.5$-in. lens. The average pulse duration $\langle\tau\rangle$ was used to convert energy to power via $P=\mathcal{E}/(\pi)^{1/2}\langle\tau\rangle$, as discussed in Sec. II D. The three circled points resulted from atypically short pulses.

commercial sources, and all except $SiO_2$ and ED-4, were monocrystalline. All results are for a geometry with the propagation direction along the [001] axis and electric vector along the [100] axis, except for the YAG: Nd material, in which the propagation direction was along a [111] axis. This sample orientation was chosen in order to measure the same quantities that are operational in YAG: Nd laser rods.

### A. Pulse-duration dependence of the breakdown threshold in NaCl

Graphs such as Fig. 5 yield the breakdown-threshold electric field according to Eq. (6), as discussed previously. Field values so obtained are independent of all self-focusing effects. The field values obtained by us are all absolute, and the experimental uncertainty, estimated by reproducibility and by calculation, is ±15%.

In this section we examine the pulse-duration dependence of the breakdown threshold in alkali halides probed by pulses of 1.06-$\mu$m radiation only. Measurements have been made in NaCl for four different pulse durations, from 10 nsec to 15 psec, by previous investigators.[2] Those data are reproduced in Fig. 6, along with the datum point for 30 psec measured by us. The solid curve in that figure is the result of an approximate theoretical calculation discussed in Ref. 2. The previous investigators described the pulse duration dependence of the

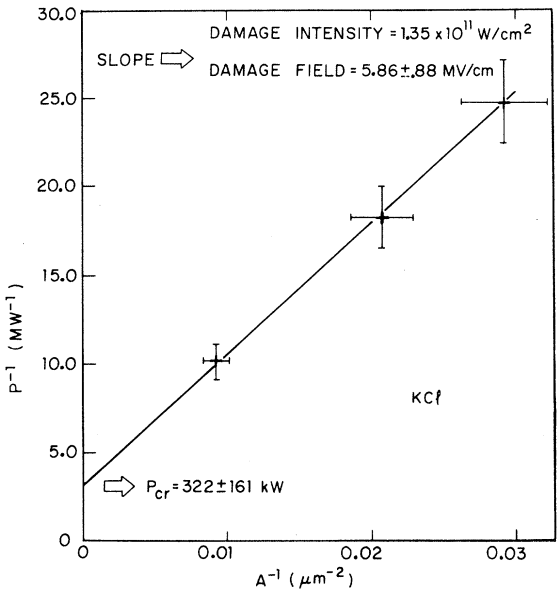


FIG. 5. Results of breakdown experiments in KCl for three lenses. The solid line is a least-squares fit to the data. The slope equals the reciprocal threshold breakdown intensity and the vertical-axis intercept equals the reciprocal critical power for self-focusing.

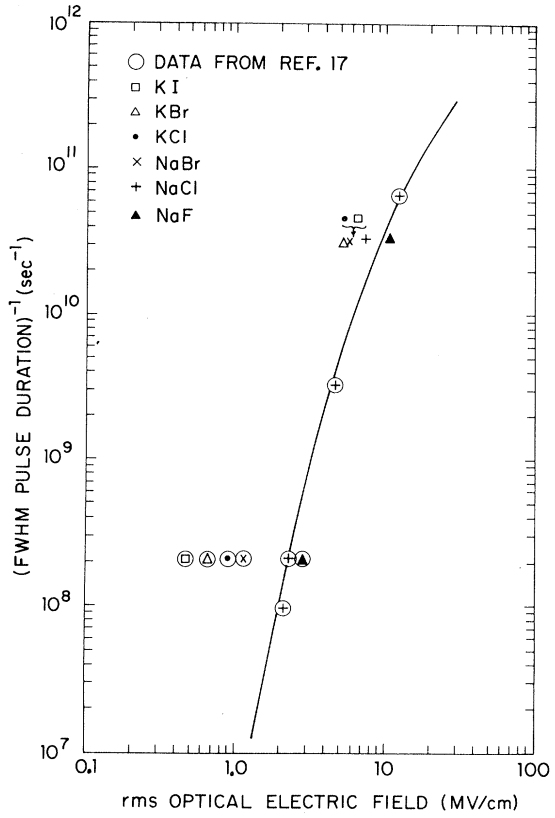


FIG. 6. Functional relationship between the breakdown threshold electric field strength and the pulse duration. The solid curve is a semiempirical prediction for NaCl, discussed in Ref. 2.

threshold in terms of a field-dependent ionization rate $\alpha(E)$, inversely proportional to the pulse width. An exponential relation between the number of conduction electrons and time was obtained

$$N(t) = N_0 \exp\left(\int_{-\infty}^{t} \alpha[E(t')]\, dt'\right) \equiv N_0 M(t) , \qquad (13)$$

where $M(t)$ describes the evolution of the initial number $N_0$ (~ $10^8$ to $10^{10}$ per cm$^3$). As mentioned earlier, because $M(t)$ must reach ~ $10^{10}$ during the presence of the laser pulse, stronger fields are necessary as the pulse duration is decreased. Therefore the field dependence of the ionization rate, as well as the pulse duration dependence of the threshold, is displayed in Fig. 6.

In addition to data for NaCl, the data now available at 1.06 $\mu$m for five other alkali halides are illustrated in Fig. 6. The three Na halides display a similar relative dependence of threshold on pulse duration, which appears to be somewhat different for the K halides. In combination with dc measurements by others,[16] the data of Fig. 6 make available the approximate field dependence of the ionization rate in six materials.

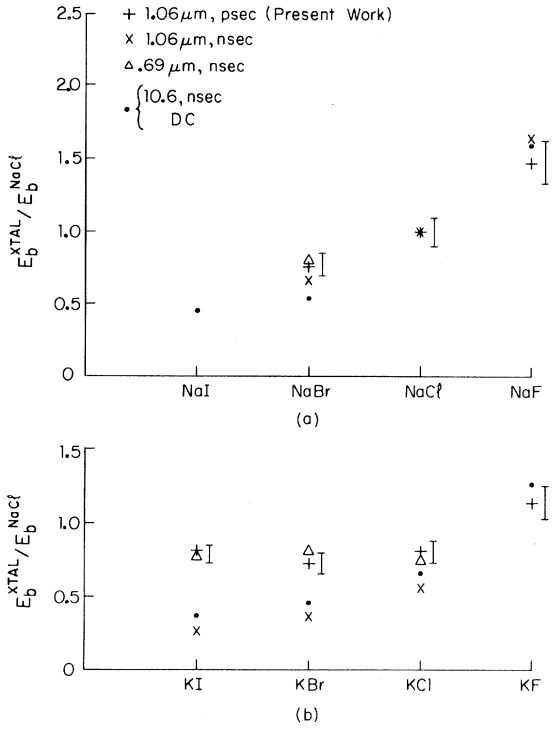


FIG. 7. Experimental trend of the breakdown field through (a) the Na halides and (b) the K halides. Shown for comparison are data from previous studies: (×), Ref. 19; (△), Ref. 18; (•), dc data from Ref. 16, 10.6-μm data from Ref. 17. In the figure nsec denotes a pulse duration the order of nanoseconds, and psec, picoseconds. Each set of data is normalized to the field for NaCl of that same data set. Error bars for the present work are shown displaced to the right.

### B. Variation of the breakdown-threshold field through the Periodic Table

We now consider the variation of the breakdown threshold among different substances for picosecond pulses at 1.06-μm wavelength. The results of our measurements are presented in Table II. The threshold is observed to vary from a minimum of 3.4 MV/cm to a maximum of 22.28 MV/cm among the materials tested. KDP possesses a threshold so high as to approach the level necessary to make multiphoton ionization probable. Figure 7 displays the trend of our threshold measurements across the Periodic Table for the Na and K halides. For comparison, previous data from dc,[16] and $Q$-switched $CO_2$,[17] ruby,[18] and YAG: Nd,[19] laser-damage studies are presented. Note that all the data for a particular combination of pulse duration and frequency are normalized to the NaCl threshold of that same data set.

### C. Third-order electronic susceptibility

The critical power for self-focusing, as given by Eqs. (2) and (6), is obtained in these experiments as the inverse of the intercept of the fitted line with the vertical axis, in graphs such as Fig. 5. The nonlinear index $n_2$ and $\chi^{(3)}(-\omega, \omega, \omega, -\omega)$ are related by

$$n_2 = 12\pi\chi^{(3)}(-\omega, \omega, \omega, -\omega)/n_0 . \quad (14)$$

The experimental condition that the laser-pulse duration is much shorter than the electrostrictive response time ($\sim 10^{-9}$ sec) and that the materials investigated are ionic solids, indicate that the values of $P_{cr}$, $n_2$, and $\chi^{(3)}$ obtained in these experiments are those of electronic ($E$) origin only. Several techniques have previously been employed to measure $\chi^{(3)E}$, among them third-harmonic generation,[20,21] three-wave mixing,[22,23] intensity-dependent ellipse rotation,[24] nonlinear birefringence,[25] and time-resolved interferometry.[26]

The values obtained in the present experiments for the critical power $P_{cr}$, the nonlinear refractive index, and the third-order electronic susceptibility $\chi^{(3)E}_{xxxx}(-\omega, \omega, \omega, -\omega)$ are presented in Sec. A of Table III. Also tabulated is the linear refractive index used to convert $n_2$ into $\chi^{(3)E}$. The experimental accuracy of $P_{cr}$, and of $\chi^{(3)E}$, is estimated to be ±50%. Section B of the table lists previously obtained values of $\chi^{(3)E}$ for comparison. The smallest $\chi^{(3)E}$ value was registered by NaF, a factor of almost 18 less than that of KBr. Agreement with previous values is substantial, except for LiF, given the rather large experimental uncertainties

TABLE II. rms breaksown electric field strengths ($E_b$ uncertainty, ±15%; field ratio uncertainty, ±10%).

| | NaF | NaCl | NaBr | KF | KCl | KBr | KI |
|---|---|---|---|---|---|---|---|
| $E_b$ (MV/cm) | 10.77 | 7.34 | 5.67 | 8.34 | 5.86 | 5.33 | 5.87 |
| $E_b/E_b^{NaCl}$ | 1.47 | 1.00 | 0.77 | 1.14 | 0.80 | 0.73 | 0.80 |

| | LiF | RbI | ED-4[a] glass | YaG:Nd | Fused $SiO_2$ | $CaF_2$ | KDP |
|---|---|---|---|---|---|---|---|
| $E_b$ (MV/cm) | 12.24 | 3.40 | 9.90 | 9.82 | 11.68 | 14.44 | 22.28 |
| $E_b/E_b^{NaCl}$ | 1.67 | 0.46 | 1.35 | 1.34 | 1.59 | 1.97 | 3.04 |

[a]Owens-Illinois (Toledo, Ohio) undoped laser glass.

TABLE III. Results for $\chi^{(3)E}_{1111}(-\omega,\omega,\omega,-\omega)$.

| | A. Present work | | | | B. $\chi^{(3)E}_{1111}$ ($10^{-14}$ esu), other work | | | | | |
|---|---|---|---|---|---|---|---|---|---|---|
| | | | | | Experiment[a] | | | | Theory[b] | |
| Material | $P_{cr}$ (MW) | $n_0$ | $n_2$ ($10^{-14}$ esu) | $\chi^{(3)E}_{1111}$ ($10^{-14}$ esu) ±50% | I ±300% | II ±20% | III | Other | I | II |
| NaBr | 0.111 | 1.62 | 96.15 | 4.13 | | | | | | |
| NaCl | 0.166 | 1.532 | 64.66 | 2.63 | 1.2 | 1.7 | | | 0.8 | 2.0 |
| NaF | 1.13 | 1.321 | 9.45 | 0.33 | 0.25 | | | | 0.13 | 0.3 |
| KI | 0.095 | 1.638 | 112.35 | 4.88 | | | | | 3.1 | 9.0 |
| KBr | 0.075 | 1.544 | 142.31 | 5.83 | 2.8 | 3.0 | | | 1.3 | 3.7 |
| KCl | 0.322 | 1.479 | 33.15 | 1.30 | 1.2 | 1.9 | | | 0.9 | 1.9 |
| LiF | 0.438 | 1.387 | 24.37 | 0.90 | 0.3 | 0.2 | $0.34\pm0.06$ | | 0.28 | 0.3 |
| $CaF_2$ | 0.389 | 1.429 | 27.70 | 1.05 | | 0.35 | $0.43\pm0.13$ | | 0.4 | 0.4 |
| fused $SiO_2$ | 0.783 | 1.450 | 13.63 | 0.52 | | 0.7 | $0.70\pm0.12$ | $0.38\pm0.03^{IV}$ | 1.4 | 1.1 |
| KDP | 0.295 | 1.494 | 36.18 | 1.43 | | | | | | |
| ED-4 | 0.503 | 1.550 | 21.22 | 0.87 | | | $1.07\pm0.08$ | $0.71\pm0.05^{IV}$ | | |
| YAG:Nd[c] | 0.302 | 1.823 | 35.34 | 1.71 | | | $2.18\pm0.13$ | $1.98\pm0.14^{IV}$<br>$1.53\pm0.30^{V}$ | | 0.62 |

[a]I. Values from third-harmonic generation, Wang and Bardeen, Ref. 20. II. Values from three-wave mixing, Maker and Terhune, Ref. 22. III. Values from three-wave mixing, Levenson and Bloembergen, Ref. 23. IV. Values from intensity-dependent ellipse rotation, Owyoung, Ref. 24. V. Values from time-resolved interferometry, Bliss *et al.*, Ref. 26.

[b]I. Calculated from generalized Miller's, $\chi^{(3)}=(\chi^{(1)})^4\times10^{-10}$ esu, Wang, Ref. 27. II. Calculated from Wang's rule, Ref. 27.

[c]All experimental values in this row, with one exception, are for pulse propagation along a [111] direction, the usual laser rod configuration. In these cases, the measured susceptibility is $\frac{1}{2}(\chi^{(3)E}_{1111}+\chi^{(3)E}_{1221}+2\chi^{(3)E}_{1122})$. The value in the column designated III is for the single element $\chi^{(3)E}_{1111}$, however. The present work investigated a YAG:Nd crystal; all other values in the row pertain to undoped YAG crystal.

listed. The only serious discrepancy occurs for LiF. The difference between our value for LiF and those obtained by others is a factor of approximately 3. We tested two different samples of LiF, a total of three times, and our results were reproducible. Therefore, we know of no reason to suspect that the error in our value for LiF exceeds the stated uncertainty of ±50%. The expected trend of the third-order susceptibility element through the periodic table is displayed for the Na and K halides.

## IV. SUMMARY

The method of controlled dielectric breakdown[6,7] has been demonstrated to be a useful way to measure simultaneously the two intrinsic parameters which must be known to enable propagation of maximum picosecond-light intensity through a material in a stable nondestructive manner. Those parameters, the breakdown field strength and the electronic nonlinear refractive index, have been measured in several materials of scientific interest with 1.06-$\mu$m laser pulses of 30-psec average duration (FWHM). The measurements were made with well-calibrated pulses and focal geometry, in a manner allowing elimination of any inclusion effect and measurement of intrinsic processes characteristic of the bulk. A simple technique was related for the measurement of (individual picosecond pulse duration)-(pulse area) products. The values of $\chi^{(3)E}(-\omega,\omega,\omega,-\omega)$ presented here are in reasonable agreement with those of other investigators. The measured breakdown field strengths have been shown to be those of an avalanche ionization process. Further picosecond experiments at the second-harmonic frequency are in progress to investigate the onset and properties of dielectric breakdown driven by multiphoton ionization.

## ACKNOWLEDGMENTS

The authors are grateful to Patrick Heck of Owens-Illinois, Inc., for supplying a sample of ED-4 glass, and to S. Maurici for his skillful preparation of the many samples. One of us (W. L. S.) is also appreciative of helpful discussions with Professor Eli Yablonovitch of Harvard.

*Research supported in part by the National Aeronautics and Space Administration, by the Joint Services Electronics Program and by the Advanced Research Projects Agency.

[1]N. Bloembergen, IEEE J. Quantum Electron. QE-10, 375 (1974).

[2]D. W. Fradin, N. Bloembergen, and J. P. Lettelier, Appl. Phys. Lett. 22, 635 (1973).

[3]S. A. Akhmonov, R. V. Khokhlov, and A. P. Sukhorukov, in *Laser Handbook*, edited by F. T. Arecchi and E. O. Schulz-DuBois (North-Holland, Amsterdam, 1972), Vol. 2, Chap. E3.
[4]J. H. Marburger (unpublished).
[5]W. G. Wagner, H. A. Haus, and J. H. Marburger, Phys. Rev. 175, 256 (1968).
[6]G. M. Zverev and V. A. Pashkov, Zh. Eksp. Teor. Fiz. 57, 1128 (1969) [Sov. Phys.-JETP 30, 616 (1970)].
[7]D. W. Fradin, IEEE J. Quantum Electron. QE-9, 954 (1973). Note that Eq. (2) in this reference should read $I_d = I_0(1 - P/P_{cr})^{-1}$.
[8]A. Feldman, D. Horowitz, and R. M. Waxler, IEEE J. Quantum Electron. QE-9, 1054 (1973).
[9]I. M. Winer, Appl. Opt. 5, 1437 (1966).
[10]P. W. Smith, M. A. Duguay, and E. P. Ippen, in *Progress in Quantum Electronics*, edited by J. H. Sanders and S. Stenholm (Pergamon, Oxford, 1974), Vol. 3, Pt. 2, Chap. 4.
[11]W. L. Smith and J. H. Bechtel (unpublished). The proportionality expressed by Eq. (8) was noted by W. H. Glenn and M. J. Brienza [Appl. Phys. Lett. 10, 221 (1967)], and used by C. V. Shank and E. P. Ippen [Appl. Phys. Lett. 24, 373 (1974)], in conjunction with a cw mode-locked dye laser.
[12]J. H. Bechtel, W. L. Smith, and N. Bloembergen, Opt. Commun. 13, 56 (1975).
[13]W. J. Smith, *Modern Optical Engineering* (McGraw-Hill, New York, 1966), Chap. 3. The lenses used in these experiments were either standard or custom products of Special Optics, Little Falls, N. J. 07424.
[14]E. Yablonovitch, thesis (Harvard University, 1972) (unpublished).
[15]P. L. Ruben, J. Opt. Soc. Am. 54, 45 (1964).
[16]A. von Hippel, J. Appl. Phys. 8, 815 (1937).
[17]E. Yablonovitch, Appl. Phys. Lett. 19, 495 (1971).
[18]D. W. Fradin and M. Bass, Appl. Phys. Lett. 22, 206 (1973).
[19]D. W. Fradin, E. Yablonovitch, and M. Bass, Appl. Opt. 12, 700 (1973).
[20]C. C. Wang and E. L. Bardsen, Phys. Rev. 185, 1079 (1969); and Phys. Rev. B 1, 2827 (1970).
[21]W. K. Burns and N. Bloembergen, Phys. Rev. B 4, 3437 (1971).
[22]P. D. Maker and R. W. Terhune, Phys. Rev. 137, A801 (1965).
[23]M. D. Levenson, IEEE J. Quantum. Electron QE-10, 110 (1974); and M. D. Levenson and N. Bloembergen, Phys. Rev. B 10, 4447 (1974).
[24]A. Owyoung, IEEE J. Quantum Electron. QE-9, 1064 (1973).
[25]M. A. Duguay and J. W. Hansen, in *Damage in Laser Materials*, Natl. Bur. Stds. Spec. Publ. No. 341 (U.S. GPO, Washington, D.C., 1970), p. 45.
[26]E. S. Bliss, D. R. Speck, and W. W. Simmons, Appl. Phys. Lett. 25, 728 (1974).
[27]C. C. Wang, Phys. Rev. B 2, 2045 (1970).